# Profiling the PM2.5 Mass Concentration Vertical Distribution in the boundary layer

Zongming Tao[1,2], Zhenzhu Wang[2,*], Shijun Yang[1], Huihui Shan[1], Xiaomin Ma [1], Hui Zhang [1], Sugui Zhao [1], Dong Liu [2], Chenbo Xie [2], Yingjian Wang [2,3]

[1]New Star Institute of Applied Technology, Hefei, Anhui 230031, China

[2]Key Laboratory of Atmospheric Composition and Optical Radiation, Anhui Institute of Optics and Fine Mechanics, Chinese Academy of Sciences, Hefei, Anhui 230031, China

[3]University of Science and Technology of China, Hefei, Anhui 230031, China

*Corresponding author: zzwang@aiofm.ac.cn

Submitting to AMT

(Version 4.0)

New method for PM2.5 profile

**Abstract:**

Fine particle (PM2.5) affects human life and activities directly; the detection of PM2.5 mass concentration profile is very essential due to its practical and scientific ~~meanings~~ significance (such as~~,~~ quantifying of air quality and its variability, and improving air quality forecast and assessment). But so far, it is difficult to detect PM2.5 mass concentration profile. The proposed methodology to study the relationship between aerosol extinction coefficient and PM2.5 mass concentration is described, which indicates that the PM2.5 mass concentration profile could be retrieved by combining a charge-coupled device (CCD) side-scatter lidar ~~and~~ with a PM2.5 sampling detector. When the relative humidity is less than 70%, PM2.5 mass concentration is proportional to the aerosol extinction coefficient, and then the specific coefficient can be calculated. ~~Using~~ Through this specific coefficient, aerosol extinction profile is converted to PM2.5 mass concentration profile. Three cases of clean night (on September 21, 2014), pollutant night (on March 17, 2014), and heavy pollutant night (on February 13, 2015) are studied. The characteristics of PM2.5 mass concentration profile in near-ground during these three nights' cases in the western suburb of Hefei city was discussed. The PM2.5 air pollutant concentration is comparatively large in close surface ~~varying~~ and varies with time and altitude. The experiment results show that the CCD side-scatter lidar combined with a PM2.5 detector is an effective and new method to explore pollutant mass concentration profile in near-ground.

## 1 Introduction

Atmospheric aerosol is defined as suspended particle in the air, and its size ~~distribution~~ distributes ~~is~~ from 0.001 μm to 100 μm in diameter in liquid or solid state. PM2.5 is a particular group of particle, whose size is less than 2.5μm in diameter, and it is an important part of aerosol. PM2.5 is also called fine particle because of its small size. PM2.5 is considered to be the most serious pollutant in the urban areas all over the world due to its adverse health effects, including cardiovascular diseases, respiratory irritation, and pulmonary dysfunction [An et al., 2000; Mai et al., 2002; Xu et al., 2007]. The PM2.5 poses ~~the~~ great health risks, compared to the coarse particle matter, because the increased surface areas have high potential to adsorb or condense toxic air pollutants [An et al., 2000]. Meanwhile PM2.5 can degrade the atmospheric visibility and affect traffic safety by the extinction effect. In recent years, a series of experiments or monitors about fine particle matter are researched in many mega cities in China by institutes [Mao et al., 2002], and the results indicated that the PM2.5 mass concentration ~~were~~ was increased.

Precise knowledge on the vertical distribution of PM2.5 is required for at least two reasons: (1) It is better for quantifying ~~of~~ air quality and its variability since, for example, the different vertical ~~location~~ distribution of PM2.5 near the earth surface ~~or not~~ has very different impact on public health; (2) It is likely to significantly enhance the PM2.5 estimation and provide data information for model evaluation, improvement, and development for daily air quality forecast.

Currently, the direct detecting device for PM2.5 is the particle matter sampling monitor, which is mostly installed on the surface ground. Using the meteorological tower, only a few researchers ~~put~~ fitted PM2.5 monitors at different altitudes in Beijing and Tianjin to get the profile of PM2.5 mass concentration within 325 m [Wu et al., 2009; Yang et al., 2005]. So it is difficult to obtain PM2.5 mass concentration profile in a few kilometers. However, some important atmospheric processes (i.e. particle formation, transportation and mixing processes) take place predominantly at a higher altitude in the planetary boundary layer. Lidar in principle can provide the ability to observe these processes where they occur. Backscattering lidar is a powerful tool to detect aerosol profile, and is widely used in atmospheric monitor [Weitkamp, 2005; Winker et al., 2007; Bo et al., 2014; Wang et al., 2014]. But the common backscattering lidar system has a shortcoming in the lower hundreds of meters because of the geometric form factor (GFF) caused by the configuration of the transmitter divergence and receiver's field-of-view (FOV) at the near range [Mao et al., 2012; Wang et al., 2015b]. With the recently developed technique of the CCD side-scattering lidar [Bernes et al., 2003; Tao et al., 2014a; Ma et al., 2014], the problem caused by the GFF could be solved. Moreover, the nearer range~~,~~ and the better spatial resolution could be obtained. So the side-scattering lidar is very suitable ~~to~~ for detecting aerosol spatial distribution in the boundary layer from the surface.

In this paper, the aerosol extinction coefficient profile is retrieved by our self-developed CCD side-scattering lidar, and PM2.5 mass concentration is measured simultaneously on the ~~in~~ ground level by a particle matter monitor. Syncretizing these

two datasets measured at the same time and in the same place, the profile of PM2.5 mass concentration can be derived in the boundary layer. In section 2, the instrumentation is introduced; and the methodology for extinction and PM2.5 profiles is shown in section 3; then the results ~~is~~ are discussed in section 4; followed by the summary and conclusion in the last section 5.

## 2 Instruments

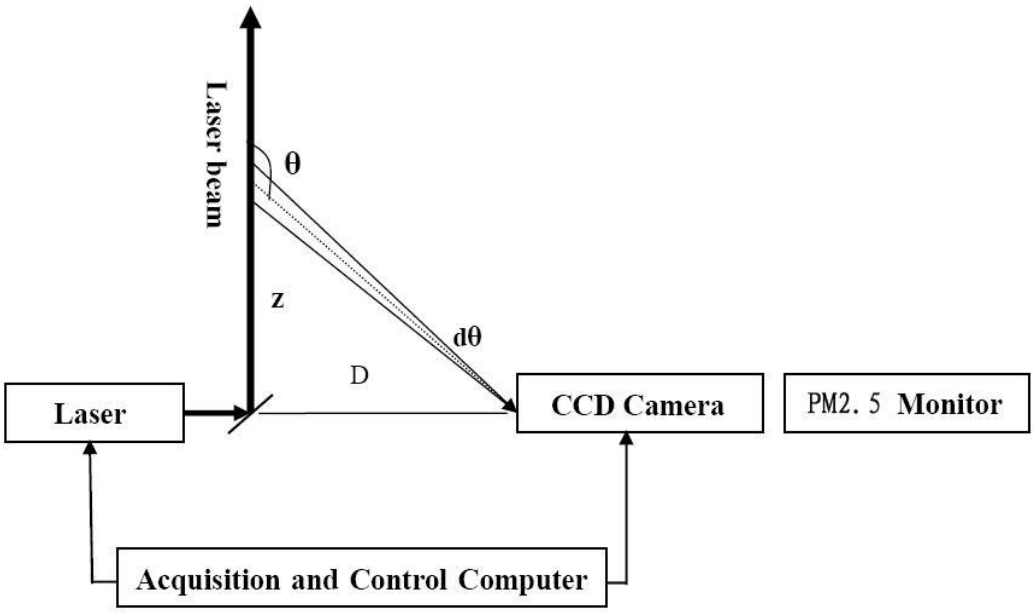


Fig. 1 The diagram of the measurement system

The measurement system ~~is~~ consists ~~ted~~ of a CCD side-scattering lidar and a PM2.5 mass monitor as shown in figure 1. The subsystem of side-scattering lidar consists of laser, CCD camera, geometric calibration, data acquisition and control computer. The light source is a Nd:YAG laser (Quantel Brilliant) emitting laser pulses in 20 Hz at 532 nm wavelength. The side-scattering light is received by a CCD camera with 3352×2532 pixels. The exposed time is set as 5 min according to the signal-to-noise

ratio with a maximum relative error of 1.5% caused by noises [Ma et al., 2014], and there is an interference filter with 30 nm bandwidth in front of CCD lens. ~~Using~~ Through geometric calibration, the relationship between the pixels and the corresponding ~~to the~~ scattering lights in laser beam is determined. The computer acquires the CCD camera data and controls timing sequence between laser and CCD camera. PM2.5 mass monitor works simultaneously~~,~~ and the output ~~product~~ is the average PM2.5 mass concentration throughout one hour. In Fig. 1~~,~~; z is the detecting distance~~,~~; D is the distance from CCD camera to laser beam~~,~~; $\theta$ is the scattering angle~~,~~; $d\theta$ is the FOV of one pixel. The detailed specifications of the CCD side-scattering lidar (C-lidar) are described in the previous work [Tao et al., 2014a] and shown in Table 1.

Table 1. The specifications of the C-lidar system

| | |
|---|---|
| Laser （Quantel Brilliant）Nd:YAG | |
| Wavelength (nm) | 532 |
| Pulse energy (mJ) | 200 |
| Repetition rate (Hz) | 20 |
| Detector （SBIG ） ST-8300M | |
| Pixel array | 3352×2532 |
| Pixel size (μm) | 5.4×5.4 |
| A/D convecter (bits) | 16 |
| Wide-angle lens | Walmexpro f/2.8 |
| Lens focal length (mm) | 14 |
| CCD sensor | Kodak KAF-8300 |
| Quantum efficiency (532nm) | ~55% |
| Interference Filter （Semrock corporation） | |
| Bandwidth (nm) | 25.6 |
| Peak transmittance | ~95% |

The PM2.5 mass monitor, named Thermo Scientific TEOM 1405 Ambient Particulate

Monitor, can carry out continuous measurement of ambient particulate concentrations with the resolution of 0.1 μg/m³ and the precision of ±2.0 μg/m³ (one hour averaged).

## 3 Methodology

### 3.1 Retrieved method of aerosol extinction profile

The side-scattering lidar equation is expressed as [Tao et al., 2014b]:

$$P(z,\theta)=\frac{P_0KA}{D}\left(\frac{\beta_1(z,\pi)}{f_1(\pi)}f_1(\theta)+\frac{\beta_2(z,\pi)}{f_2(\pi)}f_2(\theta)\right)\bullet\exp(-\tau-\tau/\cos(\pi-\theta))d\theta \quad (1)$$

Where $P(z,\theta)$ is the received power at height z and scattering angle $\theta$ by a pixel, $P_0$ is laser pulse energy, $K$ is a system constant including the optical and electronic efficiency and $A$ is the area of CCD camera lens, D is the distance from CCD camera to laser beam , $\beta(z,\pi)$ is backscattering coefficient, $f(\theta)$ is phase function. Subscripts "1" and "2" represent aerosol and molecule scattering, respectively. $\tau$ is optical depth, $\alpha(z)$ is extinction coefficient, and $\tau=\int_0^z(\alpha_1(z')+\alpha_2(z'))dz'$.

In general, for Eq. (1), there ~~is~~ are six unknown variables, i.e. phase function, backscattering and extinction coefficients of aerosol and molecule. Three unknown variables for molecule are calculated ~~from~~ through the standard molecular model ~~using~~ by Rayleigh scatter theory. A prior assumption has to be given, i.e. lidar ratio (extinction-to-backscattering ratio) of aerosol, in order to reduce an unknown. The value of 50 Sr is used as lidar ratio at 532 nm wavelength in our algorithm. The aerosol phase function is determined from a sky-radiometer (for example, a Prede POM-02 sky-radiometer made in Japan). Then only one variable (the backscattering or extinction coefficient of aerosol) is left, which can be ~~retrieved~~ derived from Eq. (1)

as follows~~ing~~.

In our experiment, vertical-pointing backscattering lidar (V-lidar) and C-lidar worked simultaneously. For V-lidar data processing, it is a traditional way to select the clear point about the tropopause as the reference point ~~where~~ assumed ~~has~~ to have minimum aerosol. The V-lidar signals and C-lidar signals have an overlap region around 1 km in height in our case. For C-lidar, the reference point is selected in this overlap region. Aerosol backscatter coefficient value $\beta_c$ at reference point thus can be given from V-lidar retrieval. When the aerosol backscatter coefficient value at the scattering angle $\theta_c$ as the reference point is known, according to Eq. (1), the backscattering or extinction coefficient of aerosol can be derived ~~by~~ in our proposed numerical inversion method [Tao et al., 2014b]. The validation experiments and error analysis are shown in the reference [Tao et al., 2015]. When comparative experiments were performed, the C-lidar and V-lidar worked at the same position simultaneously, as well as another horizontal-pointing backscattering lidar (H-lidar). The result shown in the Fig. 2 of the reference [Tao et al., 2015] indicates a good agreement and the total relative error of extinction coefficient is less than 18% accordingly ~~by applying~~ in the error propagation method and ~~taking~~ by the typical example.

### 3.2 Retrieved method of PM2.5 profile

Some researchers [Pesch et al., 2007; Sano et al., 2008; He et al., 2010; Cordero et al., 2012] studied the relationship between the PM2.5 mass concentration and aerosol optical depth ~~from the view of~~ by a review of statistics. The aerosol optical depth is the integral result of aerosol extinction to range, which may match the column PM2.5

mass concentration. However, the aerosol extinction and PM2.5 mass concentration both ~~are~~ chang~~e~~ing along altitude. So the PM2.5 mass concentration has close relation ~~with~~ to the aerosol extinction in theory.

The aerosol size distribution $n(r)$ is defined as

$$n(r) = \frac{dN}{dr} \quad (2)$$

Where $dN$ is the particle number concentration in radius interval range $(r \to r + dr)$.

Total particle matter mass concentration $C_{Total}$ can be written as

$$C_{Total} = \int_0^{\infty} \rho(\frac{4}{3}\pi r^3) n(r) dr \quad (3)$$

Where $\rho$ is the aerosol mass density.

PM2.5 mass concentration $C_{PM\,2.5}$ can be written as

$$C_{PM\,2.5} = \int_0^{2.5um} \rho(\frac{4}{3}\pi r^3) n(r) dr \quad (4)$$

Aerosol extinction coefficient $\alpha$ can be described as

$$\alpha = \int_0^{\infty} \pi r^2 Q_{ext} n(r) dr \quad (5)$$

Where $Q_{ext}$ is the factor of extinction efficiency.

The mean and integral properties of the particle ensemble that are calculated from the inverted particle size distribution are effective radius, i.e. the surface-area-weighted mean radius as

$$r_{eff} = \int_0^{\infty} r^3 n(r) dr \Big/ \int_0^{\infty} r^2 n(r) dr \quad (6)$$

So, the relationship between aerosol extinction and total particle mass concentration is ~~gotten~~ determined [Li et al., 2013]

$$\alpha = \frac{3Q_{ext}}{4r_{eff}\rho} C_{Total} \qquad (7)$$

Using the ratio of total particle matter mass concentration to PM2.5 mass concentration ($\eta = C_{Total} / C_{PM\,2.5}$), finally we got the following relationship

$$\alpha = \frac{3Q_{ext}\eta}{4r_{eff}\rho} C_{PM\,2.5} = K \cdot C_{PM\,2.5} \qquad (8)$$

Eq. (8) is the formula to convert aerosol extinction profile to PM2.5 mass concentration profile, where $K = \frac{3Q_{ext}\eta}{4r_{eff}\rho}$ is the specific coefficient.

In Eq. (8), the specific coefficient $K$ is related to aerosol size distribution, refractive index, and atmospheric relative humidity. In planetary boundary layer (PBL), due to turbulence effect, the aerosol size distribution and refractive index are assumed as uniform reasonably. When the relative humidity is below 70%, the aerosol hydrophilic growth could be negligible. So, the specific coefficient $K$ could be considered as constant under the condition of less than 70% relative humidity in PBL, i.e. $K$ is independent of altitude, though this assumption will lead to limitation.

In a measurement, the CCD side-scattering lidar and PM2.5 monitor operate ~~at~~ in the same place simultaneously. ~~Selecting~~ After the aerosol extinction coefficient value corresponding to the altitude of PM2.5 monitor and PM2.5 mass concentration value is selected, the specific coefficient $K$ is ~~got~~ determined by ~~applying~~ Eq. (8). Then us~~e~~ing Eq. (8) again, and the PM2.5 mass concentration profile could be derived from

aerosol extinction coefficient profile and the specific coefficient $K$ .

## 4 Results

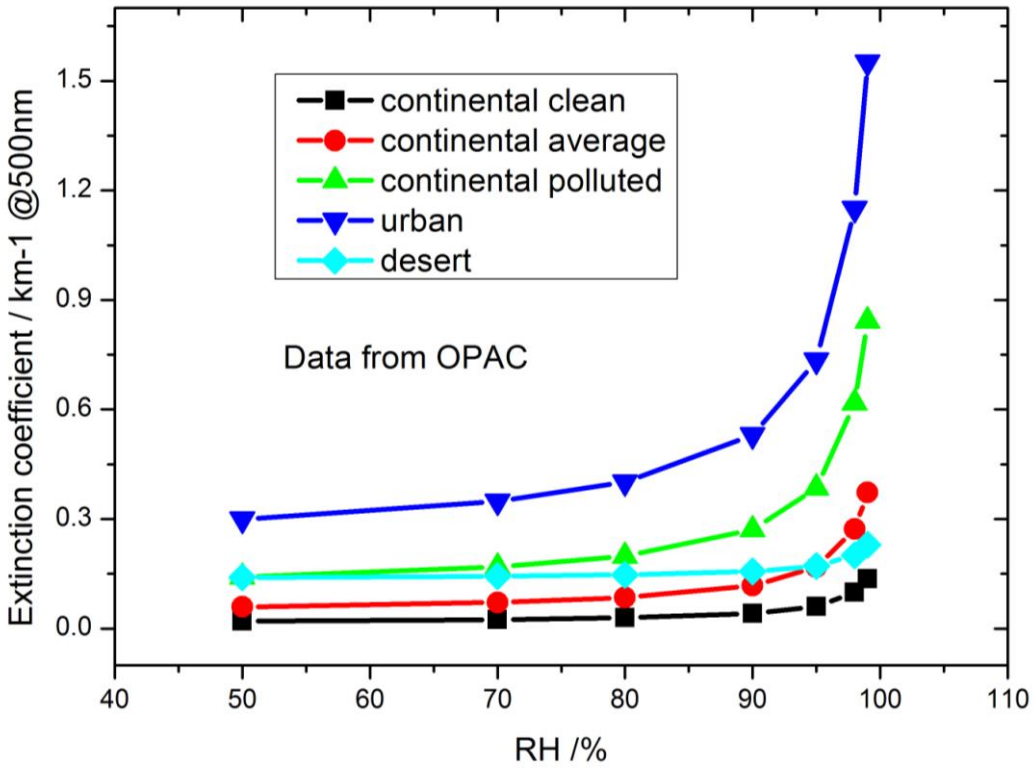


Fig. 2 the relationship between aerosol extinction coefficient and atmospheric relative humidity (RH) for five types of aerosol

Our CCD side-scattering lidar system was set up since April, 2013 in the SKYNET Hefei site. After that, the system ~~was~~ operated to detect atmospheric aerosol during cloud-free night. In the following, three cases are shown~~ed~~ to represent clean day, pollutant day, and heavy pollutant day respectively. Before this~~at~~, in order to verify the prior assumption, we investigated how the aerosol extinction coefficient is associated with the atmospheric relative humidity (RH) through numerical calculation. The selected aerosol types for the calculation are shown in Figure 2. The parameters

and components for figure 2 were from Optical Properties of Aerosols and Clouds (OPAC) 3.1 by Hess et al. [1998]. As mentioned in the previous~~e~~ literature [Wang et al., 2014; 2015a], the Hefei site is ~~situated~~ located ~~on~~ in the east of China, which is predominantly~~ted by~~ continental aerosol. The nearest urban influence is 15 km and therefore, the site is close enough to be influenced by local urban depending on wind direction. And in S~~s~~pring ~~season~~, dust aerosol ~~transported~~ from the northern/northwest regions of China may also affect this site [Zhou et al., 2002]. So, five different aerosol types are considered in figure 2 and ~~there is~~ they are rarely reliant on RH when RH is less than 70%.

### 4.1 Case I: Clean night

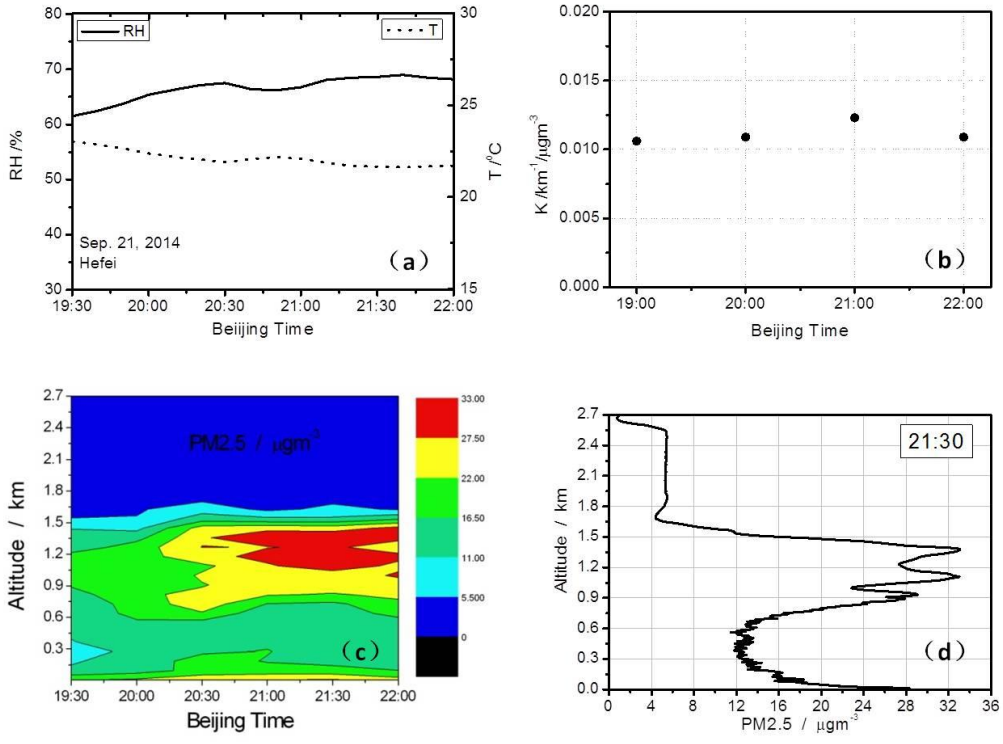


Fig. 3 (a) RH and T parameters with time, (b) K value for each hour, (c) Time series

of PM2.5 profile, and (d) Vertical distribution of PM2.5 at 21:30 BT measured in Hefei site on Sep. 21, 2014

On September 21, 2014, it was clear at night, with northeast wind of not more than 3 m/s near ground. The temperature ~~varies~~ ranges from $21.6^0$C to$23.0^0$C with a slight decreasing trend and the RH increases from 61% to 69% during the time span of 19:30-22:00 Beijing Time (BT) as shown in figure 3 (a). The distance D between laser beam and CCD camera is 34.34 m.

Figure 3 (b) plots the hourly mean value of K varying from 0.011 to 0.012 $km^{-1}/(\mu gm^{-3})$, which indicates an approximately constant value during this experimental case. ~~Using~~ With the specific coefficient K and the aerosol extinction coefficient profile, PM2.5 profile is given accordingly. Figure 3 (c) presents spatio-temporal distribution of PM2.5 mass concentration for this case in Hefei site. The PM2.5 is almost enclosed below 1.5 km above ground level (AGL) with a maximum~~s~~ value 33 $\mu gm^{-3}$, indicating a clean night in Hefei. The floating layer of 0.6-1.5 km AGL indicates a higher PM2.5, ~~whose~~ of which the value is more than that below 0.3 km AGL near the earth surface layer from figure 3 (c). The floating layer exists throughout the night due to a stable aerosol loading. There is a clean layer between the floating layer and the earth surface layer. It is noted from figure 3 (d) that the PM2.5 value decreases from 28 $\mu gm^{-3}$ ~~at~~ on the earth surface to 12 $\mu gm^{-3}$ at 0.3 km AGL, and keeps at a certain value at 0.3-0.6 km AGL, and then increases to three sub-peaks of 29, 33, and 33 $\mu gm^{-3}$ in the floating layer, respectively. The vertical distribution of PM2.5 at 21:30 BT measured in Hefei site on Sep. 21, 2014 depicts a

rich structures.

## 4.2 Case II: Pollutant night

On March 17, 2014, it was also clear at night, with the south wind of not more than 3 m/s near the earth surface. The temperature varies from $18.2^0$C to $21.7^0$C with a decreasing trend and the RH increases from 58% to 70% during the time span of 19:30-24:00 BT as shown in figure 4 (a). The distance D between laser beam and CCD camera is 23.90 m.

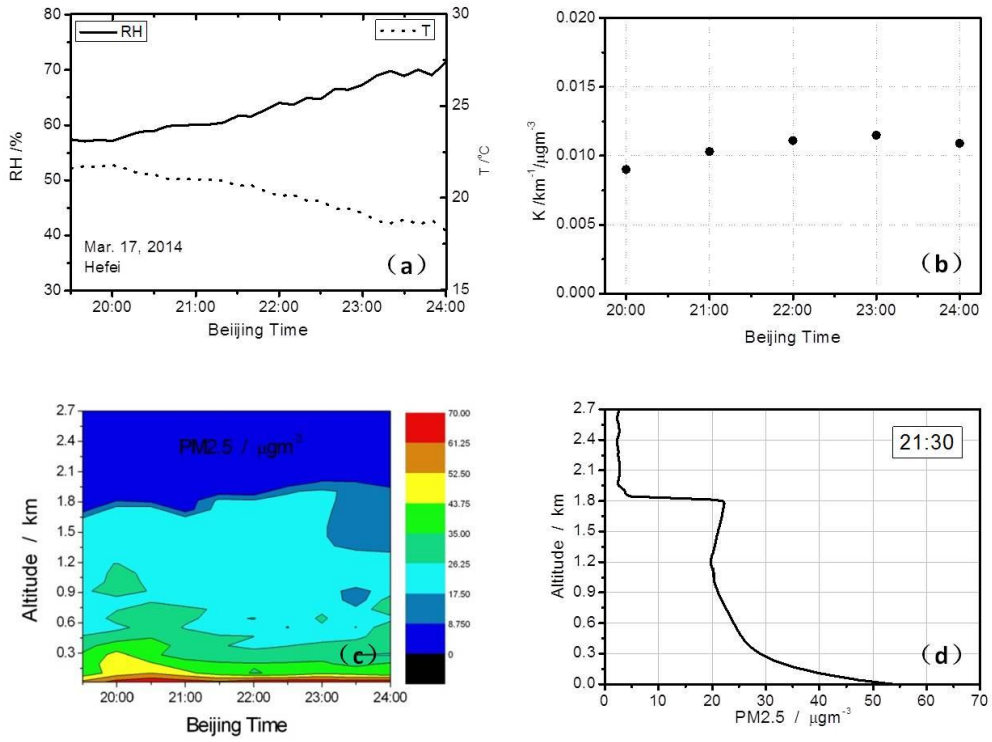


Fig. 4(a) RH and T parameters with time, (b) K value for each hour, (c) Time series of PM2.5 profile, and (d) Vertical distribution of PM2.5 at 21:30 BT measured in Hefei site on Mar. 17, 2014

Figure 4 (b) plots the hourly mean value of K varying around 0.011 $km^{-1}/(\mu gm^{-3})$ with the minimum of 0.009 and the maximum of 0.012, which also indicates an

approximately constant value during this experimental case. Then PM2.5 profile is given accordingly by ~~using~~ the specific coefficient K and the aerosol extinction coefficient profile. The spatio-temporal distribution of PM2.5 mass concentration for this case in Hefei site is shown in Figure 4 (c). The PM2.5 is almost enclosed below 1.8 km AGL with a maximum~~s~~ value of 70 $\mu gm^{-3}$, indicating a ~~light~~ mild pollutant night in Hefei. Between 0.6 km and 1.8 km AGL, the PM2.5 value is almost constant indicating a well mixed layer. The maximum value of PM2.5 lies near the earth surface layer and forms a rather stable aerosol structure, which will cause a ~~haze~~ hazy day with poor visibility.

It is ~~remarked~~ revealed in ~~from~~ figure 4 (d) that the PM2.5 value remains 20 $\mu gm^{-3}$ at 0.9-1.8 km AGL, and increases to 30 $\mu gm^{-3}$ at 0.3 km AGL, then increases rapidly to a peak of 55 $\mu gm^{-3}$ at the earth surface. The vertical distribution of PM2.5 at 21:30 BT measured in Hefei site on Mar. 17, 2014 depicts a stable structure.

### 4.3 Case III: Heavy pollutant night

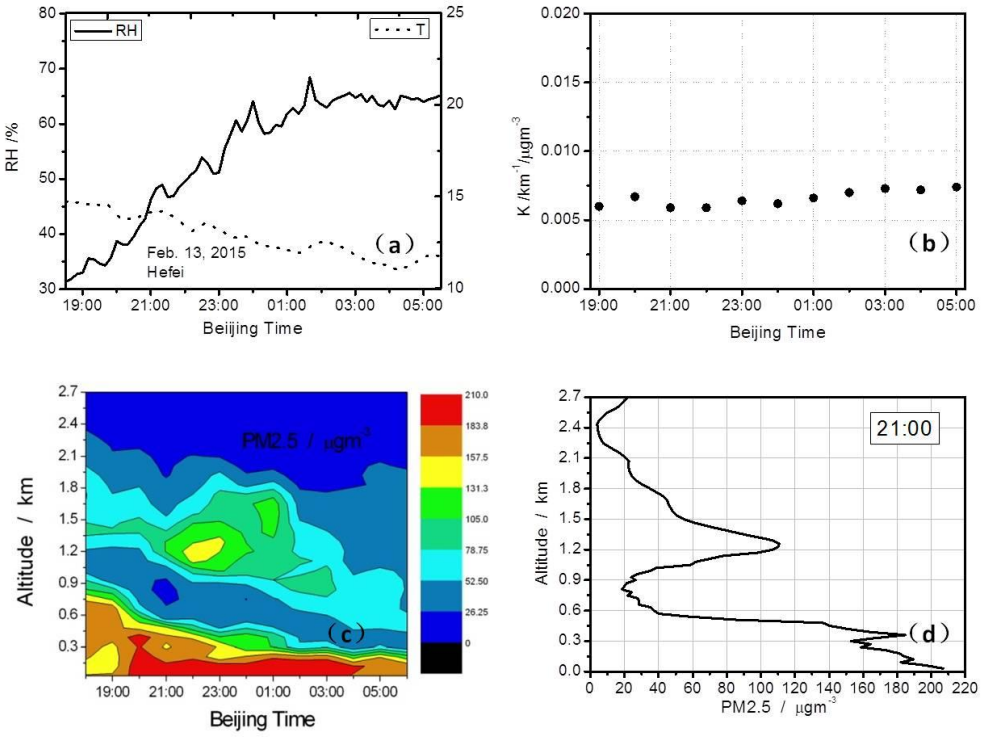


Fig. 5 (a) RH and T parameters with time, (b) K value for each hour, (c) Time series of PM2.5 profile, and (d) Vertical distribution of PM2.5 at 21:00 BT measured in Hefei site on Feb. 13-14, 2015

On February 13-14, 2015, it was also cloud-free at night, with the northwest wind of not more than 3 m/s near the ground. The temperature varies from 10.7$^0$C to 9.1$^0$C with a decreasing trend and the RH increases speedily from 31% to 68% during the time span of 18:30-02:00 BT, and then keeps around 65% in the late period of 02:00-05:30 BT as shown in figure 5 (a). The distance D between laser beam and CCD camera is 19.40 m.

Figure 5 (b) plots the hourly mean value of K varying from 0.006 to 0.007 $km^{-1}/(\mu gm^{-3})$, which also indicates an approximate constant value during this experimental case. But this value is quite different from that obtained from CASE I and CASE II ~~maybe~~ probably due to the differences ~~of~~ in aerosol size distribution and

refractive index. The PM2.5 profile is calculated accordingly by ~~using~~ the K value and the aerosol extinction coefficient profile. At the ~~meanwhile~~meantime, the spatio-temporal distribution of PM2.5 mass concentration for this case in Hefei site is shown in Figure 5 (c). The PM2.5 ~~is lifted up~~rises to 2.1 km AGL with a maximum~~s~~ value 210 $\mu gm^{-3}$, indicating a heavy pollutant night in Hefei. During the observation period, there are three distinct layers (i.e., the floating layer, the clean layer, and the earth surface layer) with a gradual fall in height from the evening to the next morning. The typical height for the floating layer decreases from 1.2-1.8 km AGL to 0.5-1.0km AGL and the peak value of PM2.5 for this layer is about 150 $\mu gm^{-3}$. The PM2.5 value for the fair layer in middle part varies from 30 to 50 $\mu gm^{-3}$. The top height of the earth surface layer decreases from 0.9 km AGL at 18:00 BT to 0.3 km AGL at 06:00 BT, which leads to a more stable structure. The maximum value of PM2.5 lies near the earth surface layer, especially below 0.3 km AGL, where a high value region of PM2.5 (i.e., 200 $\mu gm^{-3}$) exists all along from 20:00 BT to 04:00 BT, which will cause a heavy ~~haze~~ hazy day with worse visibility.

It is remarked from figure 5(d) that the PM2.5 value takes on a sub-peak of 110 $\mu gm^{-3}$ at 1.2 km AGL, and increases rapidly from 20 $\mu gm^{-3}$ at 0.8 km AGL to another sub-peak of 190 $\mu gm^{-3}$ at 0.4 km AGL, then increases rapidly again to a peak of 210 $\mu gm^{-3}$ ~~at~~ on the earth surface. The vertical distribution of PM2.5 at 21:00 BT measured in Hefei site on Feb. 13-14, 2015 ~~appears~~ forms a more stable and rich structure.

## 5 Summary and Conclusion

A new measurement technology of PM2.5 mass concentration profile in near-ground is presented in this paper based on a CCD side-scatter lidar and a PM2.5 detector. Our new method is proved to be effective through the three cases measured during nighttime in SKYNET Hefei site. And some useful conclusions are ~~summarized~~ drawn as follows~~ing~~:

1) Five types of aerosol from OPAC, prevailing in Hefei site, are used to testify their extinction property depending on RH, only to ~~find~~ indicate ~~that there is rarely reliant~~ seldom reliance on RH when RH is less than 70%.
2) The specific coefficient K, which is related to aerosol size distribution, refractive index, and atmospheric relative humidity, may contain a fixed value under the suitable condition when RH is less than 70%, though it may not be the same for each case. So, the PM2.5 mass concentration profile can be easily derived from vertical distribution of extinction coefficient for aerosol.
3) The PM2.5 is always loading in the planet boundary layer with a multi-~~layers~~ layered structure, indicating its complexity of the vertical distribution. And there is a higher lifting height under the heavy polluted weather condition, demonstrating air pollution may break through near the surface into a higher altitude and join in further transportation.
4) The high value of PM2.5 remains near the ground and forms a stable structure, especially in ~~haze~~ hazy day, which will cause ~~a~~ bad weather conditions, such as

low visibility.

5) Our new method for PM2.5 mass concentration profile is a useful approach for improving our understanding of air quality~~,~~ and atmospheric environment, which can also provide critical information for daily air quality forecast. Further investigation will be carried on in the near future when RH is larger than 70% including the potential variation of specific coefficient K.


## Acknowledgements

This research is supported by the National Natural Science Foundation of China (Nos. 41175021 ~~and~~ , 41305022 and 41590870), the Ministry of Science and Technology of China (No. 2013CB955802)~~, and the Anhui Provincial Natural Science Foundation (No. 1308085MD53)~~. We ~~would also like to thank~~ will also express our gratitude to all the anonymous reviewers for their constructive and insightful comments.


## References


An, J., Zhang, R., and Han, Z.: Seasonal changes of total suspended particles in the air of 15 big cities in northern parts of China, Climatic and Environmental Research, 5(1), 25-29, 2000.

Bernes, J. E., Bronner, S., Becket, R.: Boundary layer scattering measurements with a charge-coupled device camera lidar , Applied Optics, 42(15), 2647-2652, 2003.

Bo, G., Liu, D., and Wu, D.: Two-wavelength lidar for observation of aerosol optical

362 and hygroscopic properties in fog and haze days, Chinese Journal of Lasers, 41(1),
363 0113001, 2014.
364 Cordero, L., Wu, Y., Gross, B. M., Moshary, F.: Use of passive and active ground and
365 satellite remote sensing to monitor fine particulate pollutants on regional scales,
366 Advance environmental, chemical, and Biological sensing technologies IX, Proc. Of
367 SPIE 8366, 83660M, 2012.
368 He, X., Deng, Z., Li, C., Lau, A. K., Wang, M., Liu, X., Mao, J.: Application of
369 MIDIS AOD in surface PM10 evaluation, Acta Scientiarum Naturalium
370 Universitatis Pekinensis, 46(2), 178—184, 2010.
371 Hess, M., Koepke, P., and Schult, I.: Optical properties of aerosols and clouds: The
372 software package OPAC, Bull. Am. Meteorol. Soc., 79, 831–844, 1998.
373 Li, Q., Li, C., Wang, Y., Lin, C., Yang, D., Li, Y., Retrieval on mass concentration of
374 urban surface suspended particulate matter with lidar and satellite remote sensing,
375 Acta Scientiarum Naturalium Universitatis Pekinensis, 49(4), 673—682, 2013.
376 Ma, X.,Tao, Z., Ma, M.: The retrival of side-scatter lidar signal based on CCD
377 technique, Acta Optica Sinica, 34(2), 0201001, 2014.
378 Mao, F., Gong, W., and Li, J.: Geometrical form factor calculation using Monte Carlo
379 integration for lidar, Optics & Laser Technonolgy, 44(4): 907-912, 2012.
380 Mao, J., Zhang, J., and Wang, M.: Summary comment on research of atmospheric
381 aerosol in China, Acta Meteorologica Sinica, 60(5), 625-634, 2002.
382 Pesch, M., and Oderbolz, D.: Calibrating a ground based backscatter lidar for
383 continuous measurements of PM2.5, lidar technology, techniques, and

measurements for atmospheric remote sensing III, Proc. Of SPIE 6750, 67500K, 2007.

Sano, I., Mukai, M., Okada, Y., Mukai, S., Sugimoto, N., Matsui, I., Shimizu, A.: Improvement of PM2.5 analysis by using AOT and lidar data Remote sensing of the atmospheric and clouds Ⅱ, Proc. Of SPIE 7152, 71520M, 2008.

Tao, Z., Liu, D., and Ma, X.: Development and case study of side-scatter lidar system based on charge-coupled device, Infrared and Laser Engineering, 43(10), 3282-3286, 2014a.

Tao, Z., Liu, D., and Wang, Z.: Measurements of aerosol phase function and vertical backscattering coefficient using a charge-coupled device side-scatter lidar, Opt. Express, 22(1), DOI: 10.1364/OE.22.001127, 2014b.

Tao, Z., Liu, D., Ma, X., Shi, B., Shan, H., and Zhao, M.: Vertical distribution of near-ground aerosol backscattering coefficient measured by a ccd side-scattering lidar, Applied Physics B, 120, 631-635, 2015.

Wang, Z., Liu, D., Wang, Y., Wang, Z., and Shi, G.: Diurnal aerosol variations do affect daily averaged radiative forcing under heavy aerosol loading observed in Hefei, China, Atmos. Meas. Tech. , 8, 2901–2907, doi:10.5194/amt-8-2901-2015, 2015a.

Wang, Z., Liu, D., Wang, Z., Wang, Y., Khatri, P., Zhou, J., Takamura, T., and Shi, G.: Seasonal characteristics of aerosol optical properties at the SKYNET Hefei site (31.90 °N, 117.17 °E) from 2007 to 2013, J. Geophys. Res. Atmos., 119, 6128–6139, doi:10.1002/2014JD021500, 2014.

406 Wang, Z., Tao, Z., Liu, D., Wu, D., Xie, C., and Wang, Y.: New experimental method
407 for lidar overlap factor using a CCD side-scatter technique, Opt. Lett., 40,
408 1749-1752, 2015b.
409 Wang, Z., Liu, D., Cheng, Z.: Pattern recognition model for haze identification with
410 atmospheric backscatter lidars, Chinese Journal of Lasers, 41(11), 1113001, 2014.
411 Weitkamp, C.: Lidar: Range-Resolved Optical Remote Sensing of the Atmosphere,
412 Springer, New York, 2005.
413 Winker, D., Hunt, W., and McGill, M.: Initial performance of assessment of CALIOP,
414 Geophysics Research Letter, 34(19), L19803, 2007.
415 Wu., Z., Liu, A., and Zhang, C.: Vertical distribution feature of PM2.5 and effect of
416 boundary layer in Tianjin, Urban Environment & Urban Ecology, 22(4), 24-29,
417 2009.
418 Xu, J., Ding, G., and Yan, P.: Componential characteristics and sources identification
419 of PM2.5 in Beijing, Journal of Applied Meteorological Science, 18(5), 645-654,
420 2007.
421 Yang, L., He, K., and Zhang, Q.: Vertical distributive characters of PM2.5 at the
422 ground layer in Autumn and Winter in Beijing, Research of Environmental Sciences,
423 18(2), 23-28, 2005.
424 Zhou, J., Yu, G., Jin, C., Qi, F., Liu, D., Hu, H., Gong, Z., Shi, G., Nakajima, T., and
425 Takamura, T.: Lidar observations of Asian dust over Hefei, China, in spring 2000, J.
426 Geophys. Res., 107, AAC5.1–AAC5.8, doi:10.1029/2001JD000802, 2002.
427